Letter

Search for rare decays $B^+ \to D_s^{(*)+}\eta$, $D_s^{(*)+}\bar{K}^0$, $D^+\eta$, and D^+K^0

M. Kumar, V. Bhardwaj, K. Lalwani, I. Adachi, H. Aihara, D. M. Asner, T. Aushev, V. Babu, P. Behera, K. Belous, J. Bennett, M. Bessner, B. Bhuyan, T. Bilka, A. Bobrov, D. Bodrov, G. Bonvicini, J. Borah, A. Bozek, M. Bračko, P. Branchini, T. E. Browder, A. Budano, M. Campajola, D. Červenkov, M.-C. Chang, P. Chang, B. G. Cheon, K. Chilikin, H. E. Cho, K. Cho, S.-J. Cho, S.-K. Choi, Y. Choi, S. Choudhury, D. Cinabro, S. Das, N. Dash, G. De Pietro, R. Dhamija, F. Di Capua, J. Dingfelder, Z. Doležal, T. V. Dong, D. Dossett, D. Epifanov, D. Ferlewicz, B. G. Fulsom, R. Garg, V. Gaur, A. Garmash, A. Giri, P. Goldenzweig, E. Graziani, T. Gu, Y. Guan, K. Gudkova, C. Hadjivasiliou, T. Hara, K. Hayasaka, H. Hayashii, W.-S. Hou, C.-L. Hsu, T. Iijima, K. Inami, N. Ipsita, A. Ishikawa, R. Itoh, M. Iwasaki, W. W. Jacobs, E.-J. Jang, Q. P. Ji, S. Jia, Y. Jin, K. K. Joo, D. Kalita, K. H. Kang, C. Kiesling, C. H. Kim, D. Y. Kim, K.-H. Kim, Y.-K. Kim, K. Kinoshita, P. Kodyš, A. Korobov, S. Korpar, E. Kovalenko, P. Križan, P. Krokovny, R. Kumar, K. Kumara, Y.-J. Kwon, T. Lam, J. S. Lange, M. Laurenza, S. C. Lee, C. H. Li, J. Li, L. K. Li, Y. Li, Y. B. Li, L. Li Gioi, J. Libby, K. Lieret, D. Liventsev, M. Masuda, T. Matsuda, D. Matvienko, S. K. Maurya, F. Meier, M. Merola, F. Metzner, K. Miyabayashi, R. Mizuk, G. B. Mohanty, M. Mrvar, I. Nakamura, M. Nakao, Z. Natkaniec, A. Natochii, L. Nayak, M. Nayak, N. K. Nisar, S. Nishida, S. Ogawa, H. Ono, P. Oskin, P. Pakhlov, G. Pakhlova, S. Pardi, H. Park, S.-H. Park, A. Passeri, S. Patra, S. Paul, T. K. Pedlar, R. Pestotnik, L. E. Piilonen, T. Podobnik, E. Prencipe, M. T. Prim, M. V. Purohit, N. Rout, G. Russo, S. Sandilya, A. Sangal, L. Santelj, V. Savinov, G. Schnell, J. Schueler, C. Schwanda, Y. Seino, K. Senyo, M. E. Sevior, M. Shapkin, C. Sharma, C. P. Shen, J.-G. Shiu, J. B. Singh, E. Solovieva, M. Starič, Z. S. Stottler, J. F. Strube, M. Sumihama, T. Sumiyoshi, M. Takizawa, U. Tamponi, K. Tanida, F. Tenchini, K. Trabelsi, T. Tsuboyama, M. Uchida, Y. Unno, S. Uno, R. van Tonder, G. Varner, K. E. Varvell, A. Vinokurova, E. Waheed, E. Wang, M.-Z. Wang, X. L. Wang, M. Watanabe, S. Watanuki, O. Werbycka, J. Wiechczynski, E. Won, B. D. Yabsley, W. Yan, S. B. Yang, J. Yelton, J. H. Yin, C. Z. Yuan, Y. Yusa, Y. Zhai, Z. P. Zhang, V. Zhilich, and V. Zhukova

(The Belle Collaboration)

(Received 1 September 2022; accepted 17 January 2023; published 16 February 2023)

We present a study of rare decay modes $B^+ \to D_s^+ h^0$, $B^+ \to D_s^{*+} h^0$, and $B^+ \to D^+ h^0$, where h^0 denotes the neutral meson η or K^0, using a data sample of $(772 \pm 10) \times 10^6$ $B\bar{B}$ events produced at the $\Upsilon(4S)$ resonance. The data were collected by the Belle detector operating at the asymmetric-energy KEKB collider. We find no evidence for these decays, so we set upper limits at the 90% confidence level on the branching fractions of $B^+ \to D_s^+ h^0$, $D_s^{*+} h^0$, and $D^+ h^0$ decay modes. Along with these rare decay modes, we report improved measurements of the color-suppressed decay branching fractions $\mathcal{B}(\bar{B}^0 \to D^0\eta) = (26.6 \pm 1.2 \pm 2.1) \times 10^{-5}$ and $\mathcal{B}(\bar{B}^0 \to D^0\bar{K}^0) = (5.6 \pm 0.5 \pm 0.2) \times 10^{-5}$. The first and second quoted uncertainties are statistical and systematic, respectively.

DOI: 10.1103/PhysRevD.107.L031101

The dominant amplitude for the decay $B^+ \to D_s^+ \bar{K}^0$ is expected to be the weak-annihilation process, where the initial-state $\bar{b}u$ pair annihilates to produce a virtual W^+ boson as shown in Fig. 1(a). Such annihilation amplitudes cannot be evaluated using the factorization approach [1]. The weak-annihilation amplitude is expected to be proportional to f_B/m_B, where m_B and f_B are the mass and decay constant of B meson, respectively. Numerically, $f_B/m_B \approx \lambda^2$ [1,2], where $\lambda \equiv \sin\theta_c \approx 0.22$ [3] with θ_c being the Cabibbo angle. These processes are additionally suppressed by the Cabibbo-Kobayashi-Maskawa factor $|V_{ub}| \sim \lambda^3$ [4] and so the resulting amplitudes are naively of the order of λ^5. Therefore, in most theoretical calculations such amplitudes are neglected. However, rescattering effects from other decay modes might increase the branching fractions of decays dominated by the weak annihilation [2].

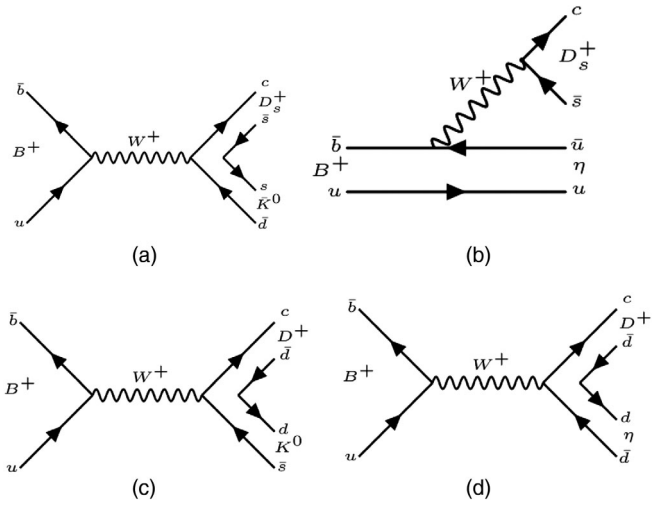

FIG. 1. Feynman diagrams for (a) $B^+ \to D_s^+ \bar{K}^0$ annihilation amplitude, (b) $B^+ \to D_s^+ \eta$ spectator amplitude, (c) $B^+ \to D^+ K^0$ annihilation amplitude, and (d) $B^+ \to D^+ \eta$ annihilation amplitude.

The related decay $B^+ \to D_s^+ \eta$, the leading process involves a $b \to u$ quark-level transition as shown in Fig. 1(b), which is suppressed by a factor $|V_{ub}|$. Searching for these decay modes is crucial in order to improve the theoretical understanding, as they provide an insight into the internal dynamics of the B mesons [1]. These rare decays are sensitive probes for physics beyond the Standard Model and are not well measured. Such measurements provide a benchmark to search for new physics contributions in loop-dominated processes that would constrain the unitarity triangle. Further, these modes also represent a significant background source for analyses of other rare modes. The decays $B^+ \to D^+ K^0$ and $B^+ \to D^+ \eta$ are of interest as these modes are also dominated by the weak-annihilation diagram as shown in Figs. 1(c) and 1(d).

The upper limits on the branching fractions of $B^+ \to D_s^{(*)+} \eta$ and $B^+ \to D_s^{(*)+} \overline{K^0}$ decays were set at the 90% confidence level by the CLEO Collaboration using a sample of 1.16×10^6 $B\bar{B}$ events [5]. In addition, the *BABAR* Collaboration reported an upper limit on $B^+ \to D^+ K^0$ decays based on a sample of 226×10^6 $B\bar{B}$ [6]. The $B^+ \to D^+ \eta$ decay mode has never been searched for. To validate the rare decay modes, we use $\bar{B}^0 \to D^0 \eta$ as a control mode for $B^+ \to D_s^+ \eta$, $D_s^{*+} \eta$, $D^+ \eta$ decay modes and $\bar{B}^0 \to D^0 \bar{K}^0$ as a control mode for study of the $B^+ \to D_s^+ \bar{K}^0$, $D_s^{*+} \bar{K}^0$, and $D^+ K^0$ decay modes. These control modes were earlier studied by Belle [7,8] and *BABAR* [9,10] using samples containing between 85×10^6 and 454×10^6 $B\bar{B}$ events.

In this Letter, we present studies of the branching fraction of rare decay modes $B^+ \to D_s^+ \eta$, $B^+ \to D_s^{*+} \eta$, $B^+ \to D_s^+ \bar{K}^0$, $B^+ \to D_s^{*+} \bar{K}^0$, $B^+ \to D^+ \eta$, and $B^+ \to D^+ K^0$; where $D_s^{*+} \to D_s^+ \gamma$; $D_s^+ \to \phi \pi^+, \bar{K}^{*0} K^+, K_S^0 K^+$; $D^+ \to K^- \pi^+ \pi^+, K_S^0 \pi^+$; and $\eta \to \gamma\gamma, \pi^- \pi^+ \pi^0$. We also report improved measurements of the branching fractions of color-suppressed decay modes $\bar{B}^0 \to D^0 \eta$ and $\bar{B}^0 \to D^0 \bar{K}^0$; where $D^0 \to K^- \pi^+$, $K^- \pi^+ \pi^+ \pi^-$, $K_S^0 \pi^- \pi^+$, and $K^- \pi^+ \pi^0$. Charge conjugate decay modes are included throughout the Letter unless explicitly stated otherwise. The results are based on the full sample of 772×10^6 B meson pairs collected by the Belle detector at the KEKB asymmetric-energy $e^+ e^-$ collider [11]. The first sample of 152×10^6 $B\bar{B}$ events was collected with a 2.0 cm radius beam pipe and a three-layer silicon detector, while the remaining 620×10^6 $B\bar{B}$ pairs were collected with a 1.5 cm radius beam pipe, a four-layer silicon detector, and modified drift chamber [12].

The Belle detector is a large-solid-angle spectrometer, which includes a silicon vertex detector, a 50-layer central drift chamber (CDC), an array of aerogel threshold Cherenkov counters (ACC), time-of-flight scintillation counters (TOF), and an electromagnetic calorimeter (ECL) comprising 8736 CsI(Tl) crystals located inside a superconducting solenoid coil that provides a 1.5 T magnetic field. An iron flux-return yoke located outside the coil is instrumented to detect K_L^0 mesons and muons. Further details of the Belle experiment can be found elsewhere [13].

To validate the analysis procedure, determine efficiencies, and study backgrounds, we use samples of simulated data generated with EVTGEN [14] with QED final-state radiation generated by PHOTOS [15]. The detector response is incorporated using GEANT3 [16]. For background studies, we use five separate simulation samples that include $e^+ e^- \to B\bar{B}$ and $q\bar{q}$ $(q = u, d, s, c)$ events. Each such sample has the same size as the data sample. We perform the analysis using the B2BII software package [17], which converts Belle data into a format compatible with the Belle II software framework [18].

We select tracks consistent with originating from the interaction point by requiring $d_r < 0.5$ and $|d_z| < 4.0$ cm, where d_r and d_z are the track impact parameters in the plane transverse and parallel to the beam axis, respectively. Particle identification of $K^\pm$ ($\pi^\pm$) candidates is accomplished by combining the information from various subdetectors: ionization energy loss from the CDC, the number of photoelectrons from the ACC, and timing measurements from the TOF. We require the likelihood ratio $\mathcal{L}(K/\pi) = \mathcal{L}_K/(\mathcal{L}_K + \mathcal{L}_\pi)$ to be greater than 0.2 (less than 0.8) for $K^\pm$ ($\pi^\pm$) candidates, where $\mathcal{L}(h)$ is the likelihood of a track being consistent with the particle h. The efficiency for kaon (pion) identification ranges between 85% and 90% (87%–91%) depending on the track momentum with the misidentification rate of a pion (kaon) as a kaon (pion) of about 11%–16% (13%–6%).

For photons, we use the ECL clusters that have energy greater than 50, 100, and 150 MeV in the barrel $(32.2° < \theta < 128.7°)$, forward $(12.4° < \theta < 31.4°)$, and backward $(130.7° < \theta < 155.1°)$ regions of the ECL,

respectively. To suppress misreconstructed $\eta \to \gamma\gamma$ candidates, we select photon candidates whose energies in the c.m. frame are greater than 300 MeV. After implementing the energy requirement on photons, the signal loss fraction is 19.6%, while the background rejection fraction is 56.3%. For photon candidates coming from D_s^{*+}, we select only those whose energies in the c.m. frame are greater than 110 MeV.

We require $\pi^0 \to \gamma\gamma(\eta \to \gamma\gamma)$ candidates to have an invariant mass $M_{\gamma\gamma}$ within the range [0.115, 0.155] ([0.50, 0.58]) GeV/c^2, which corresponds to $\pm 3\sigma$ about the nominal mass of the π^0 (η) meson [19], with σ being the mass resolution. We also reconstruct $\eta \to \pi^+\pi^-\pi^0$ candidates, which are required to have an invariant mass in the range $[0.535, 0.560]$ GeV/c^2. The mass interval corresponds to $\pm 3\sigma$ about the known η mass [19]. For the selected η and π^0 candidates, a mass-constrained fit is performed to improve the momentum resolution.

We reconstruct K_S^0 candidates by combining pairs of oppositely charged particles compatible with originating from a common vertex; both charged particles are assumed to be pions. Further, a multivariate algorithm is used to improve the purity of the sample [20]. The K_S^0 candidates are required to have an invariant mass in the range $[0.487, 0.508]$ GeV/c^2, which corresponds to $\pm 3\sigma$ about the nominal mass of the K_S^0 meson [19]. We retain only the ϕ ($\bar{K}^{*0}$) candidates having invariant masses within 14 (100) MeV/c^2 of their known values [19].

The invariant masses of the D_s^+ candidates are required to be within 13, 15, and 17 MeV/c^2 of the D_s^+ nominal mass [19] for $\phi\pi^+$, $\bar{K}^{*0}K^+$, and $K_S^0K^+$ decay modes, respectively. The invariant mass of D^+ candidates is required to be within 15 MeV/c^2 of the nominal mass of the D^+ [19] mesons for both $K^-\pi^+\pi^+$ and $K_S^0\pi^+$ decay modes. These selection criteria correspond to approximately a $\pm 3\sigma$ window. The D_s^{*+} candidates are selected from combinations of the D_s^+ and a photon. We require D_s^{*+} candidates to have ΔM between 0.13 and 0.16 GeV/c^2, where ΔM is the difference between the reconstructed mass of D_s^{*+} and D_s^+. The invariant mass of D^0 meson candidates are required to be within 20, 15, 20, and 35 MeV/c^2 of the D^0 [19] nominal mass for $K^-\pi^+$, $K^-\pi^+\pi^+\pi^-$, $K_S^0\pi^-\pi^+$, and $K^-\pi^+\pi^0$ decay modes, respectively. These selection requirements correspond to a $\pm 3\sigma$ window in mass resolution. To reduce the combinatorial backgrounds that include a poorly reconstructed π^0 candidate in the $D^0 \to K^-\pi^+\pi^0$ decay mode, we use π^0 candidates with c.m. frame momenta greater than 0.4 GeV/c and invariant masses in the range $[0.120, 0.145]$ GeV/c^2.

The B^+ and $\bar{B}^0$ meson decays are reconstructed from D_s^+, D_s^{*+}, D^+, and D^0 mesons that are combined with an η or a K_S^0 candidate. For the reconstruction of B candidates, we utilize two kinematic variables: the energy difference $\Delta E = E_B - E_{\rm beam}$, where $E_{\rm beam}$ is the beam energy and E_B is the B candidate energy, both calculated in the c.m. frame; and the beam-constrained mass $M_{\rm bc} = \sqrt{(E_{\rm beam}/c^2)^2 - (\vec{p}_B/c)^2}$, where $\vec{p}_B$ is the momentum of the B meson candidate in the c.m. frame. The resolution of $M_{\rm bc}$ is between 2.6 and 4.3 MeV/c^2 for all decay modes. The resolution of ΔE depends upon the number of photons in the final state. Candidates satisfying the $|\Delta E| < 0.18$ GeV and $M_{\rm bc} > 5.27$ GeV/c^2 criteria are retained for further consideration. The ΔE interval is kept wide for two reasons: to take care of the asymmetric signal shape in modes containing an η and to model peaking backgrounds effectively. Vertex- and mass-constrained fits are performed on intermediate candidates, such as D_s^+, D^0, ϕ, and K_S^0, while only vertex-constrained fits are performed on B^+, $\bar{B}^0$, and $\bar{K}^{*0}$ candidates. These kinematic fits result in an improved determination of the energy and momenta of the candidate B mesons.

The production cross section of $e^+e^- \to q\bar{q}$ is approximately 3 times that of $B\bar{B}$ production at energies close to the $\Upsilon(4S)$ resonance, making the continuum background suppression necessary in all modes of interest. In the c.m. frame, continuum events generally have particles collimated into back-to-back jets, whereas the particles from the nearly-at-rest B mesons produced in $B\bar{B}$ events are isotropically distributed over the full solid angle. Therefore, we combine event-shape variables and flavor-tagging information using a multivariate classifier FastBDT [21] to distinguish between continuum and $B\bar{B}$ events. The FastBDT algorithm uses the following seven variables: two modified Fox-Wolfram moments [22], the absolute value of the cosine of the angle between the thrust axis of the B candidate and that of the rest of the event in the c.m. frame, the thrust value of the signal B candidate particles, the CLEO cone [23] in 10° of the thrust axis of the B candidate, the absolute value of the cosine of the angle between the B candidate momentum and the beam axis in the c.m. frame, and the B meson category-based flavor-tagger output [24]. The Belle II flavor taggers are multivariate algorithms that receive track-hit and charged-particle identification information about particles as kinematic input on the tag side and provide the flavor of the tag-side B meson. These flavor-tagger variables provide additional discrimination in our study to separate $B\bar{B}$-like events from $q\bar{q}$ events.

The continuum background peaks at zero and signals at one in the distribution of FastBDT classifier output (C). We do not find any correlation between C and ΔE. We require candidates to have $C > 0.92$; this criterion is optimized by maximizing the figure of merit defined in Ref. [25] and retains 52%, 40%, 55%, and 47% of signal events, while removing approximately 98% of background events, for $B^+ \to D_s^+\eta$, $B^+ \to D_s^+K_S^0$, $B^+ \to D^+\eta$, and $B^+ \to D^+K_S^0$ decays, respectively. We use the Boosted Decision Trees classifiers trained on the signal modes for our study of control modes to validate and calibrate the selection.

TABLE I. The mass resolution (σ_i) of D_s^+, D^+, D^0, and $M_{\rm bc}$ used to estimate the χ^2 variable.

Mass resolution (MeV/c^2) for reconstructed decays			
$\sigma_{D_s^+}$	$D_s^+ \to \phi\pi^+$	$D_s^+ \to \bar{K}^{*0}K^+$	$D_s^+ \to K_S^0K^+$
	3.8	4.0	5.1
σ_{D^+}	$D^+ \to K^-\pi^+\pi^+$		$D^+ \to K_S^0\pi^+$
	4.7		5.1
σ_{D^0}	$D^0 \to K^-\pi^+$	$D^0 \to K^-\pi^+\pi^+\pi^-$	$D^0 \to K^-\pi^+\pi^0$
	$D^0 \to K_S^0\pi^+\pi^-$		
	6	5	12
$\sigma_{M_{\rm bc}}$	$B^+ \to D_s^+\eta$	$B^+ \to D_s^+K_S^0$	$B^+ \to D_s^{*+}\eta$
	$B^+ \to D^+\eta$	$B^+ \to D^+K_S^0$	$B^+ \to D_s^{*+}K_S^0$
	2.9	2.6	4.3

After the reconstruction, 0.9%–11% of events contain multiple B candidates, depending on the decay modes. When there are more than one B candidate in a given event, we select the best candidate (BCS) with the smallest value of $\chi^2_{\rm BCS}$, defined as

$$\chi^2_{\rm BCS} = \chi^2_{M_{\rm bc}} + \chi^2_{M_i}, \tag{1}$$

where the $\chi^2_{M_i}$ variable is calculated using the reconstructed mass M_i, its resolution σ_i, and the corresponding nominal mass m_i [19] of the reconstructed meson i as $\chi^2_{M_i} = (\frac{M_i - m_i}{\sigma_i})^2$, and i indicates a D_s^+, D^+, and D^0 meson. Table I summarizes the resolution (σ_i) of $D^+_{(s)}$, D^0, and $M_{\rm bc}$ used to estimate $\chi^2_{M_i}$. The BCS chooses the correctly reconstructed B candidate between 57% and 70% of the time, depending on the decay mode.

In $B^+ \to D^+\eta$ ($B^+ \to D^+K_S^0$), the peaking background at $\Delta E \sim -0.16$ GeV comprises candidates reconstructed from $\bar{B}^0 \to D^+\rho^-$ ($\bar{B}^0 \to D^+K^{*-}$) decay modes. For the control mode, the significant cross feed contributions come from $\bar{B}^0 \to D^{*0}h$ to the $\bar{B}^0 \to D^0h$ decay mode at $\Delta E \sim -0.16$ GeV since the additional photon is not reconstructed. Another peaking background at around $\Delta E \sim -0.16$ GeV in the distributions of $\bar{B}^0 \to D^0\eta$ and $\bar{B}^0 \to D^0K_S^0$ decays arises from charged B meson decays into three final-state particles and $B^+ \to D^0K^{*+}$ decay modes, respectively.

All aforementioned D subdecay modes are used to reconstruct B candidates except for $\bar{B}^0 \to D^0\eta$, where we exclude the $D^0 \to K^-\pi^+\pi^0$ subdecay mode because of the large combinatorial background. The branching fractions of decay modes are extracted from the unbinned maximum-likelihood fits to the ΔE distributions. For all decay modes, the ΔE fit is performed in the range $|\Delta E| < 0.18$ GeV. For $B^+ \to D_s^+\eta$, $B^+ \to D^+\eta$, and $\bar{B}^0 \to D^0\eta$ decay modes, the signal probability density function (PDF) shape in the ΔE distribution is parametrized with the sum of a Gaussian and a bifurcated Gaussian function with a common mean. For $B^+ \to D_s^+K_S^0$, $B^+ \to D^+K_S^0$, and $\bar{B}^0 \to D^0K_S^0$ decay modes, the signal shape is modeled with the sum of two Gaussians with a common mean. The combinatorial background, mainly from continuum events, is modeled with a straight line. The peaking background at $\Delta E \sim -0.16$ GeV from partially reconstructed B decays is modeled with the sum of two Gaussian functions with a common mean. We fix all the parameters of the signal PDF for $B^+ \to D_s^+h$, $B^+ \to D_s^{*+}h$, $B^+ \to D^+h$, and $\bar{B}^0 \to D^0h$ decay modes from the corresponding simulated signal sample after applying a correction for differences between data and simulation in the mean and resolution; the corrections are estimated from the respective control modes. The peaking-background PDF parameters are also fixed to those fit to the generic simulated sample corrected for any resolution and bias with respect to the data as estimated from the control sample. A simultaneous fit is performed for $\eta \to \gamma\gamma$ and $\eta \to \pi^-\pi^+\pi^0$ decay modes for η modes in order to account for resolution differences. The projections of fits to the ΔE distribution are shown in Fig. 2.

We calculate the branching fraction using

$$\mathcal{B} = \frac{N_s}{N_{B\bar{B}} \times \mathcal{B}(\eta/K_S^0) \times \sum_i [\epsilon_{{\rm corr}_i} \times \mathcal{B}_i]}, \tag{2}$$

where N_s is the signal yield from combined D meson subdecay modes, $N_{B\bar{B}}$ is the number of $B\bar{B}$ events from the data sample [$(772 \pm 10) \times 10^6$] [13], $\mathcal{B}_i$ is the branching fraction of secondary decays reported in Ref. [19], and $\epsilon_{{\rm corr}_i}$ is the corrected signal efficiency, where i indicates the different D subdecay modes. Equation (2) assumes an equal production of neutral and charged B mesons from $\Upsilon(4S)$. Table II summarizes the corrected efficiency of the signal modes, as well as the control decay modes.

Table III summarizes the yield from the fit, signal significance, and branching fraction obtained from the combined D_s^+, D^+, and D^0 subdecay modes from the fitted distributions of ΔE; the first and second uncertainties are statistical and systematic, respectively. The signal significance ($\mathcal{S}$) is computed as $\mathcal{S} = \sqrt{2(\ln \mathcal{L}(N_s) - \ln \mathcal{L}(N_s = 0))}$, where $\mathcal{L}(N_s)$ is the likelihood of the nominal fit and $\mathcal{L}(N_s = 0)$ is the value obtained after repeating the fit with the signal yield (N_s) fixed to zero. In the absence of a significant yield for signal decay modes, an upper limit (U.L.) is set on each signal yield at the 90% confidence level (C.L.) using a frequentist approach [26], which includes systematic uncertainties. We perform pseudoexperiments by generating the fixed background from the final PDF and varying the yield of the input signal. We use the corresponding PDF that has been used to fit data for generating the datasets for pseudoexperiments. The fraction of pseudoexperiments with a fitted yield greater than the estimated signal yield in data has been taken as the

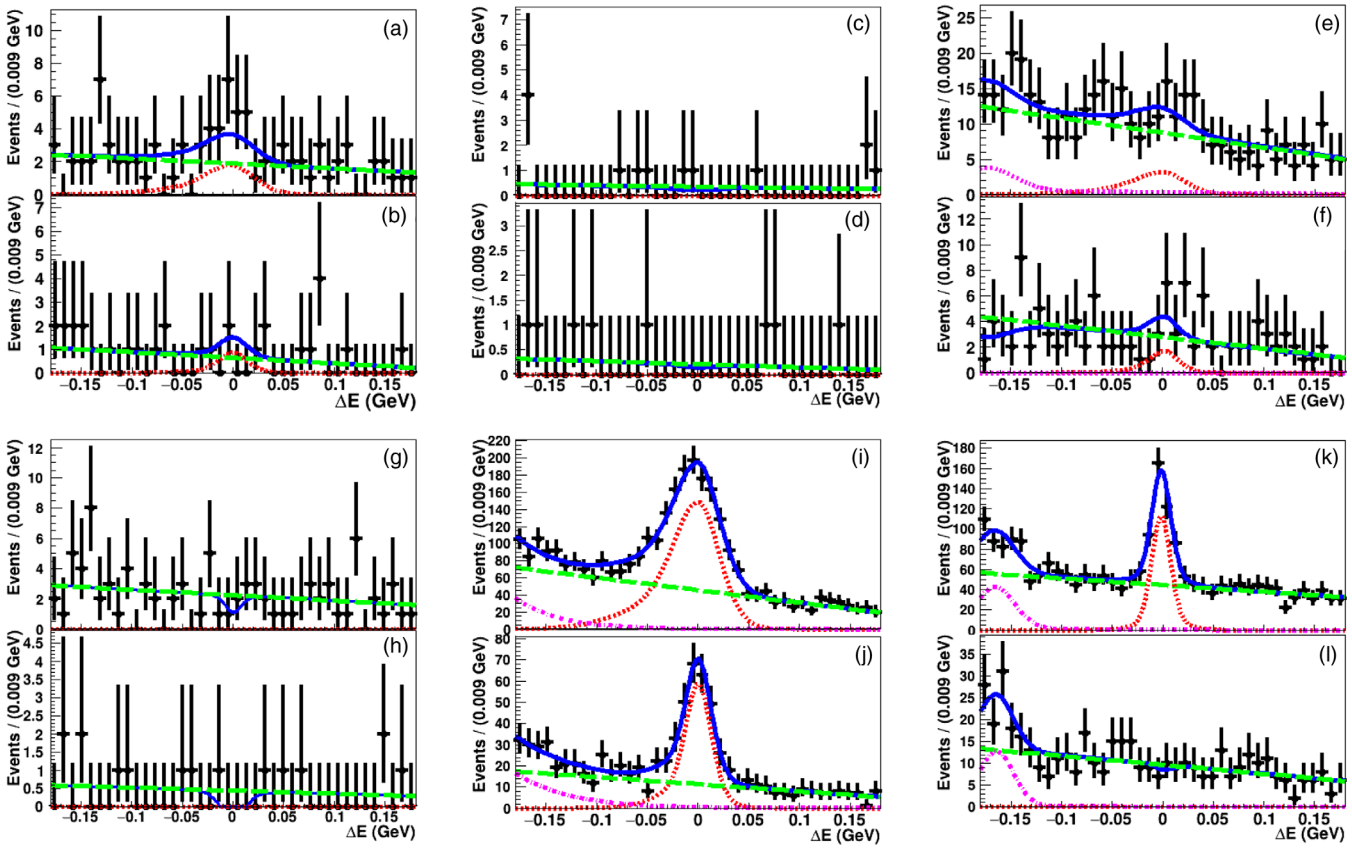

FIG. 2. Fits to the ΔE distributions in data for decay modes (a) $B^+ \to D_s^+\eta(\gamma\gamma)$, (b) $B^+ \to D_s^+\eta(\pi^-\pi^+\pi^0)$, (c) $B^+ \to D_s^{*+}\eta(\gamma\gamma)$, (d) $B^+ \to D_s^{*+}\eta(\pi^-\pi^+\pi^0)$, (e) $B^+ \to D^+\eta(\gamma\gamma)$, (f) $B^+ \to D^+\eta(\pi^-\pi^+\pi^0)$, (g) $B^+ \to D_s^+K_S^0$, (h) $B^+ \to D_s^{*+}K_S^0$, (i) $\bar{B}^0 \to D^0\eta(\gamma\gamma)$, (j) $\bar{B}^0 \to D^0\eta(\pi^-\pi^+\pi^0)$, (k) $\bar{B}^0 \to D^0K_S^0$, and (l) $B^+ \to D^+K_S^0$. A simultaneous fit is performed for $\eta \to \gamma\gamma$ and $\eta \to \pi^-\pi^+\pi^0$ decay modes. The black points with error bars show the data points. The different curves correspond to the various fit components: the solid blue curve is the total PDF, the dotted red line is the signal PDF, the dash-dotted magenta line is the peaking background PDF, and the green dashed line is the combinatorial background PDF.

TABLE II. Summary of the corrected efficiency (%) for the signal and the control decay modes.

Mode	$D_s^+(\phi\pi^+)$	$D_s^+(\bar{K}^{*0}K^+)$	$D_s^+(K_S^0K^+)$
$B^+ \to D_s^+\eta(\gamma\gamma)$	5.9	6.4	6.7
$B^+ \to D_s^+\eta(\pi^-\pi^+\pi^0)$	3.1	3.1	3.8
$B^+ \to D_s^{*+}\eta(\gamma\gamma)$	1.8	1.4	1.2
$B^+ \to D_s^{*+}\eta(\pi^-\pi^+\pi^0)$	0.9	0.7	0.7
$B^+ \to D_s^+K_S^0$	7.7	9.4	9.7
$B^+ \to D_s^{*+}K_S^0$	2.3	2.0	1.6

	$D^+(K^-\pi^+\pi^+)$	$D^+(K_S^0\pi^+)$
$B^+ \to D^+\eta(\to \gamma\gamma)$	8.1	7.8
$B^+ \to D^+\eta(\to \pi^-\pi^+\pi^0)$	4.1	4.5
$B^+ \to D^+K_S^0$	12.3	13.0

	$K^-\pi^+$	$K^-\pi^+\pi^+\pi^-$	$K_S^0\pi^+\pi^-$	$K^-\pi^+\pi^0$
$\bar{B}^0 \to D^0\eta(\gamma\gamma)$	10.0	5.6	5.8	3.0
$\bar{B}^0 \to D^0\eta(\pi^-\pi^+\pi^0)$	5.4	3.0	3.0	…
$\bar{B}^0 \to D^0K_S^0$	15.5	8.7	8.4	4.6

confidence level. We also smear the yield in the toys using systematic uncertainties.

Table IV summarizes the systematic uncertainties due to various sources. The dominant source in signal decay modes is the uncertainty on the current world-average values of the secondary decay (D_s^+, D^+, ϕ, $\bar{K}^{*0}$, K_S^0, η)

TABLE III. Summary of the fitted results. Signal yield from the ΔE fit, significance ($\mathcal{S}$) with systematic included, and measured $\mathcal{B}$; U.L. at 90% C.L., where no significant signal is observed. The first (second) uncertainties are statistical (systematic).

Decay mode	Yield (U.L.)	$\mathcal{S}$	$\mathcal{B} \times 10^{-5}$
$B^+ \to D_s^+\eta$	$18.4 \pm 7.7(21)$	1.2	<1.4
$B^+ \to D_s^{*+}\eta$	-1.45 ± 2.3 (5.5)	…	<1.7
$B^+ \to D^+\eta$	34 ± 16 (41)	1.4	<1.2
$B^+ \to D_s^+\bar{K}^0$	-2.71 ± 2.8 (4)	…	<0.3
$B^+ \to D_s^{*+}\bar{K}^0$	-2.64 ± 1.6 (1.8)	…	<0.6
$B^+ \to D^+K^0$	-2.99 ± 5.7 (8)	…	<0.2
$\bar{B}^0 \to D^0\eta$	1373 ± 63	24.7	$26.6 \pm 1.2 \pm 2.1$
$\bar{B}^0 \to D^0\bar{K}^0$	323 ± 27	14.9	$5.6 \pm 0.5 \pm 0.2$

TABLE IV. Systematic uncertainties on pion identification (π), kaon identification (K), tracking, $N_{B\bar{B}}$, K_S^0 reconstruction, η (π^0) reconstruction, photon detection, uncertainty in secondary $\mathcal{B}$, and PDF used for signal extraction.

	Uncertainty (%)										
Decay mode	π	K	Tracking	$N_{B\bar{B}}$	K_S^0	η (π^0)	γ	Secondary $\mathcal{B}$	Signal extraction PDF	Fit bias	Total
$B^+ \to D_s^+\eta$	0.8	1.1	1.2	1.4	0.2	4.1	⋯	2.0	0.5	8.4	9.8
$B^+ \to D_s^{*+}\eta$	1.1	1.6	1.2	1.4	0.2	4.1	3.0	2.2	$+4.4, -4.0$	23.2	$+24.4, -24.3$
$B^+ \to D^+\eta$	1.4	0.5	1.2	1.4	0.1	4.1	⋯	1.6	$+9.7, -12.1$	4.1	$+11.6, -13.7$
$B^+ \to D_s^+K_S^0$	0.3	0.7	1.8	1.4	1.6	⋯	⋯	1.9	1.2	2.2	4.3
$B^+ \to D_s^{*+}K_S^0$	0.4	0.9	1.8	1.4	1.6	⋯	3.0	2.1	1.2	9.9	11.0
$B^+ \to D^+K_S^0$	0.6	0.3	1.8	1.4	1.5	⋯	⋯	1.5	1.2	1.3	3.6
$\bar{B}^0 \to D^0\eta$	1.4	0.7	1.2	1.4	0.1	5.7	⋯	2.0	$+4.4, -4.0$	0.6	$+7.9, -7.7$
$\bar{B}^0 \to D^0K_S^0$	0.8	0.5	1.7	1.4	1.5	2.0	⋯	1.9	1.2	0.4	4.1

branching fractions [19]. The uncertainties related to the PDF shapes are obtained by varying all fixed parameters by $\pm 1\sigma$ and taking the change in the yield as the systematic uncertainty. The systematics uncertainty from kaon (pion) identification is estimated from a dedicated $D^{*+} \to D^0(K^-\pi^+)\pi^+$ sample, which is used to correct for the small difference in the signal detection efficiency between simulation and data for the signal decay modes. The uncertainty from $N_{B\bar{B}}$ is 1.4%. The uncertainty on the track finding efficiency is found to be 0.35% per track. The uncertainties in reconstruction efficiencies of photon and $\eta(\pi^0)$ are 3.0% [27] and 4.1% [28] per particle, respectively. The uncertainty from K_S^0 reconstruction is between 0.1% and 1.6%, which is estimated from the calibration factor derived from $D^{*\pm} \to D^0(K_S^0\pi^0)\pi^\pm_{\rm slow}$ [29]. The biases of 0.4%–23.2% observed from simplified simulated experiments are also taken as systematics related to the fitting procedure.

In summary, we have searched for $B^+ \to D_s^+h^0$, $B^+ \to D_s^{*+}h^0$, and $B^+ \to D^+h^0$ decays using the full $\Upsilon(4S)$ data sample recorded by the Belle experiment. In the absence of a significant signal yield, an upper limit at the 90% confidence level is given for each signal decay mode. We present the first search result for the $B^+ \to D^+\eta$ decay mode. The obtained upper limits are 20 times more stringent than the previous one. We report the most precise measurement to date of the branching fraction for the $\bar{B}^0 \to D^0\bar{K}^0$ [8,10] decay, which supersedes the previous Belle result [8]. The branching fraction measurement of $\bar{B}^0 \to D^0\eta$ decay modes is consistent with the world average and supersedes the previous Belle [7] result.

This work, based on data collected using the Belle detector, which was operated until June 2010, was supported by the Ministry of Education, Culture, Sports, Science, and Technology (MEXT) of Japan, the Japan Society for the Promotion of Science (JSPS), and the Tau-Lepton Physics Research Center of Nagoya University; the Australian Research Council including Grants No. DP180102629, No. DP170102389, No. DP170102204, No. DE220100462, No. DP150103061, No. FT130100303; Austrian Federal Ministry of Education, Science and Research (FWF) and FWF Austrian Science Fund No. P 31361-N36; the National Natural Science Foundation of China under Contracts No. 11675166, No. 11705209, No. 11975076, No. 12135005, No. 12175041, No. 12161141008; Key Research Program of Frontier Sciences, Chinese Academy of Sciences (CAS), Grant No. QYZDJ-SSW-SLH011; Project No. ZR2022JQ02 supported by Shandong Provincial Natural Science Foundation; the Ministry of Education, Youth and Sports of the Czech Republic under Contract No. LTT17020; the Czech Science Foundation Grant No. 22-18469S; Horizon 2020 ERC Advanced Grant No. 884719 and ERC Starting Grant No. 947006 "InterLeptons" (European Union); the Carl Zeiss Foundation, the Deutsche Forschungsgemeinschaft, the Excellence Cluster Universe, and the VolkswagenStiftung; the Department of Atomic Energy (Project Identification No. RTI 4002) and the Department of Science and Technology of India; the Istituto Nazionale di Fisica Nucleare of Italy; National Research Foundation (NRF) of Korea Grants No. 2016R1-D1A1B-02012900, No. 2018R1-A2B-3003643, No. 2018R1-A6A1A-06024970, No. RS-2022-00197659, No. 2019R1-I1A3A-01058933, No. 2021R1-A6A1A-03043957, No. 2021R1-F1A-1060423, No. 2021R1-F1A-1064008, No. 2022R1-A2C-1003993; Radiation Science Research Institute, Foreign Large-size Research Facility Application Supporting project, the Global Science Experimental Data Hub Center of the Korea Institute of Science and Technology Information and KREONET/GLORIAD; the Polish Ministry of Science and Higher Education and the National Science Center; the Ministry of Science and Higher Education of the Russian Federation, Agreement No. 14.W03.31.0026, and the HSE University Basic Research Program, Moscow; University of Tabuk research Grants No. S-1440-0321, No. S-0256-1438, and No. S-0280-1439 (Saudi Arabia);

the Slovenian Research Agency Grants No. J1-9124 and No. P1-0135; Ikerbasque, Basque Foundation for Science, Spain; the Swiss National Science Foundation; the Ministry of Education and the Ministry of Science and Technology of Taiwan; and the U.S. Department of Energy and the National Science Foundation. These acknowledgements are not to be interpreted as an endorsement of any statement made by any of our institutes, funding agencies, governments, or their representatives.

We thank the KEKB group for the excellent operation of the accelerator, the KEK cryogenics group for the efficient operation of the solenoid, and the KEK computer group and the Pacific Northwest National Laboratory (PNNL) Environmental Molecular Sciences Laboratory (EMSL) computing group for strong computing support, and the National Institute of Informatics and Science Information NETwork 6 (SINET6) for valuable network support.

[1] A. J. Buras and L. Silvestrini, Nucl. Phys. **B569**, 3 (2000).
[2] B. Blok, M. Gronau, and J. L. Rosner, Phys. Rev. Lett. **78**, 3999 (1997).
[3] L. Wolfenstein, Phys. Rev. Lett. **51**, 1945 (1983).
[4] N. Cabibbo, Phys. Rev. Lett. **10**, 531 (1963); M. Kobayashi and T. Maskawa, Prog. Theor. Phys. **49**, 652 (1973).
[5] J. P. Alexander *et al.* (CLEO Collaboration), Phys. Lett. B **319**, 365 (1993).
[6] B. Aubert *et al.* (*BABAR* Collaboration), Phys. Rev. D **72**, 011102 (2005).
[7] S. Blyth *et al.* (Belle Collaboration), Phys. Rev. D **74**, 092002 (2006).
[8] P. Krokovny *et al.* (Belle Collaboration), Phys. Rev. Lett. **90**, 141802 (2003).
[9] J. P. Lees *et al.* (*BABAR* Collaboration), Phys. Rev. D **84**, 112007 (2011).
[10] B. Aubert *et al.* (*BABAR* Collaboration), Phys. Rev. D **74**, 031101 (2006).
[11] S. Kurokawa and E. Kikutani, Nucl. Instrum. Methods Phys. Res., Sect. A **499**, 1 (2003), and other papers included in the volume; T. Abe *et al.*, Prog. Theor. Exp. Phys. **2013**, 03A001 (2013), and following articles up to 03A011.
[12] Z. Natkaniec *et al.* (Belle SVD2 Group), Nucl. Instrum. Methods Phys. Res., Sect. A **560**, 1 (2006).
[13] A. Abashian *et al.* (Belle Collaboration), Nucl. Instrum. Methods Phys. Res., Sect. A **479**, 117 (2002); also see detector section in J. Brodzicka *et al.*, Prog. Theor. Exp. Phys. **2012**, 04D001 (2012).
[14] D. J. Lange, Nucl. Instrum. Methods Phys. Res., Sect. A **462**, 152 (2001).
[15] E. Barberio and Z. Wąs, Comput. Phys. Commun. **79**, 291 (1994).
[16] R. Brun *et al.*, GEANT 3.21, CERN Program Library Long Writeup W5013 (unpublished).
[17] M. Gelb *et al.*, Comput. Software Big Sci. **2**, 9 (2018).
[18] T. Kuhr *et al.* (Belle II Framework Software Group), Comput. Softw. Big Sci. **3**, 1 (2019).
[19] P. A. Zyla *et al.* (Particle Data Group), Prog. Theor. Exp. Phys. **2020**, 083C01 (2020), and 2021 update.
[20] H. Nakano, Ph.D. thesis, Tohoku University, 2014, Chapter 4, http://hdl.handle.net/10097/58814.
[21] T. Keck, Comput. Software Big Sci. **1**, 2 (2017).
[22] The Fox-Wolfram moments were introduced in G. C. Fox and S. Wolfram, Phys. Rev. Lett. **41**, 1581 (1978); The Fisher discriminant used by Belle, based on modified FoxWolfram moments (SFW), is described in K. Abe (Belle Collaboration), Phys. Rev. Lett. **87**, 101801 (2001); Phys. Lett. B **511**, 151 (2001).
[23] D. M. Asner *et al.* (CLEO Collaboration), Phys. Rev. D **53**, 1039 (1996).
[24] Belle II Collaboration, Eur. Phys. J. C **82**, 283 (2022).
[25] G. Punzi, eConf C **030908**, MODT002 (2003).
[26] G. J. Feldman and R. D. Cousins, Phys. Rev. D **57**, 3873 (1998).
[27] N. J. Joshi *et al.* (Belle Collaboration), Phys. Rev. D **81**, 031101 (2010).
[28] M. C. Chang *et al.* (Belle Collaboration), Phys. Rev. Lett. **98**, 131803 (2007).
[29] N. Dash *et al.* (Belle Collaboration), Phys. Rev. Lett. **119**, 171801 (2017).